Design of wide-gap fluoride heterostructures for deep ultraviolet optical devices

Riadh El Ouenzerfi,[a] Shingo Ono, Alex Quema, Masahiro Goto, Masahiro Sakai, and Nobuhiko Sarukura
Institute for Molecular Science, Myodaiji, Okazaki 444-8585, Japan

Takeshi Nishimatsu, Noriaki Terakubo, Hiroshi Mizuseki, and Yoshiyuki Kawazoe
Institute for Materials Research, Tohoku University, Aoba-ku, Sendai 980-8577, Japan

Hiroki Sato, Dirk Ehrentraut, Akira Yoshikawa, and Tsuguo Fukuda
Institute of Multidisciplinary Research for Advanced Materials, Tohoku University, 2-1-1 Katahira, Aoba-ku, Sendai 980-8577, Japan

(Received 2 April 2004; accepted 30 August 2004)

The design of fluoride-based optical devices for deep ultraviolet applications is discussed. Variations in the band-gap energy and band structure with respect to composition are investigated for $Li_{(1-x)}K_xBa_{(1-y)}Mg_yF_3$ perovskites. The band-gap energy, lattice constant, and band structure of perovskitelike fluorides are estimated based on *ab initio* calculations within the local-density approximation. The lattice-matched double heterostructure with direct band-gap compounds ($Li_{(1-x)}K_xBa_{(1-y)}Mg_yF_3$ on either $LiBaF_3$ or $KMgF_3$ substrates) is promising for fabrication. © *2004 American Institute of Physics*. [DOI: 10.1063/1.1808474]

I. INTRODUCTION

Although the potential of deep ultraviolet (DUV) devices has been recognized for a long time and although the absorption edge of the electronic excited states of various promising inorganic dielectric materials and organic compounds occur in this region, technology for producing economical devices is relatively undeveloped. A large variety of real-world applications of DUV photons may emerge for material analysis, chemical reaction control, and material processing. Thus far, the complexity and high cost of light sources and optical devices in this wavelength region have obstructed progress in this direction. In the history of DUV optical devices, continuous and tremendous efforts have been made to develop shorter wavelength lasers and its coherent radiation. Devices based on capillary-discharged materials with helium, deuterium lamps, and synchrotron radiations have played important roles. With respect to the higher order harmonics of high-peak intensity lasers,[1] gas lasers, which include a F_2 laser that operates at $\lambda=157$ nm[2,3] and the sixth harmonics of $Nd:YVO_4$ lasers that use the KBBF crystal to double the third harmonics, are the sole high-output power light sources until now.[4–6] $Nd:LaF_3$ is known to operate at $\lambda=172$ nm with a F_2 laser pumping.[7,8] Some of these systems are acceptable as scientific tools, but the systems must be simplified in order to expand the applicability to other fields. The technological base for DUV devices that satisfy all of these demands might be the current injection-type semiconductor devices. This was demonstrated with III-V compound semiconductor optical devices that emit in the near infrared region.[9] In the past two decades, a continuous effort has been made in wide band-gap solid-state optical devices for the short wavelength region and include zinc-selenide-based II-VI compound semiconductor,[10] gallium nitride (GaN),[11] diamond,[12] and zinc oxide (ZnO).[13] As demonstrated for III-V compound semiconductors,[9] controlling the band gap, lattice constant, and doping are very important criteria for flexibility in designing these devices. Among these materials, diamond has the widest band gap of 5.5 eV ($\lambda=235$ nm),[12] but neither the band gap nor the lattice constant is tunable.[14,15] This significant drawback is a strongly limiting factor. To overcome this limitation, new material systems must be explored. One of the most promising candidates could be among the fluorides. From the *ab initio* calculations using the local-density approximation (LDA), Nishimatsu *et al.*[16] predicted that it should be possible to select the crystal structure, band-gap energy, band structure, and substrate crystal with the appropriate lattice constant from the wide range of complex fluorides. Moreover, growing high-quality bulk compound fluoride crystals for potential applications in lithographic optics using F_2 lasers has been successfully demonstrated in $LiCaAlF_6$ (Ref. 17), $KMgF_3$ (Refs. 18 and 19), and $LiBaF_3$.[20]

We suggested a laser diode structure that is constituted of $LiBa_xCa_ySr_{(1-x-y)}F_3$ on a $LiSrF_3$ substrate operating below $\lambda=180$ nm.[21] Despite the advantage of a large band gap, the major difficulty of this system is the availability of substrate crystals. As a possible solution to overcome this difficulty, $Li_{(1-x)}K_xBa_{(1-y)}Mg_yF_3$ is now proposed. In this paper, we report the design of a double-heterostructure laser diode based on either $KMgF_3$ or $LiBaF_3$ as a substrate operating at $\lambda=200$ nm.

II. MATERIALS

To determine a suitable composition among the $Li_{(1-x)}K_xBa_{(1-y)}Mg_yF_3$ solid solution, knowledge about the band structure, the band-gap energy, and the lattice constant

[a]Electronic mail: ouenzerf@tagen.tohoku.ac.jp

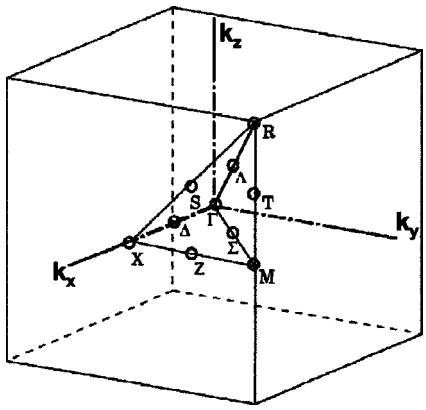

FIG. 1. First Brillouin zone in a cubic lattice.

of the perovskitelike $LiBaF_3$, $LiMgF_3$, $KBaF_3$, and $KMgF_3$ are needed. The band-gap energy and band structure are determined by *ab initio* calculations using LDA, as reported by Nishimatsu *et al.*[16] Although LDA slightly underestimates the width of band gaps, it typically provides reliable values for the band dispersions of a given material. The lattice constants of the studied compounds are estimated by the total-energy minimum and are used for each band calculation.[22] In addition, data from literature are also adopted when available.

III. RESULTS AND DISCUSSION

For cubic perovskitelike fluorides, the band structure is predicted along the symmetry lines in the first Brillouin zone, as depicted in Fig. 1. The wave vector $\vec{k}$ symmetry permits the Γ, R, Δ,… valleys to be determined.[23] Figures 2(a)–2(d) show the band structure near the band gaps of $KBaF_3$, $LiBaF_3$, $KMgF_3$, and $LiMgF_3$. For $LiBaF_3$, [Fig. 2(b)], both the conduction-band minimum and the valence-band maximum correspond to the Γ valleys. Thus, the band gap is direct. In contrast, the conduction-band minimum of $KBaF_3$, $KMgF_3$, and $LiMgF_3$ in Figs. 2(a), 2(c), and 2(d), respectively, corresponds to the Γ valley, whereas the valence-band maximum corresponds to the Δ, R, and R valleys, respectively. Consequently, the band gap is indirect. Table I represents the band-gap energy, band structure, and lattice constant for $LiBaF_3$, $LiMgF_3$, $KBaF_3$, and $KMgF_3$.

The variations in both the band-gap energy and lattice constant, as a function of the composition, are investigated in an analogous study on semiconductor compound lasers previously reported by Sasaki *et al.*[9] This study was performed using the formulae for mixed semiconductors proposed by Thompson and Woolley.[24] For $Li_{(1-x)}K_xBa_{(1-y)}Mg_yF_3$ perovskitelike fluoride, the band-gap energy can be written as follows:

$$E^{\Gamma,R,\Delta}_{Li_{(1-x)}K_xBa_{(1-y)}Mg_yF_3} = E^{\Gamma,R,\Delta}_{Li_{(1-x)}K_xMgF_3}y + E^{\Gamma,R,\Delta}_{Li_{(1-x)}K_xBaF_3}(1-y) - \frac{\alpha_{Li_{(1-x)}K_xBa_{(1-y)}Mg_yF_3}}{\sqrt{\frac{E^{\Gamma,R,\Delta}_{Li_{(1-x)}K_xMgF_3} + E^{\Gamma,R,\Delta}_{Li_{(1-x)}K_xBaF_3}}{2}}}y(1-y), \quad (1)$$

where

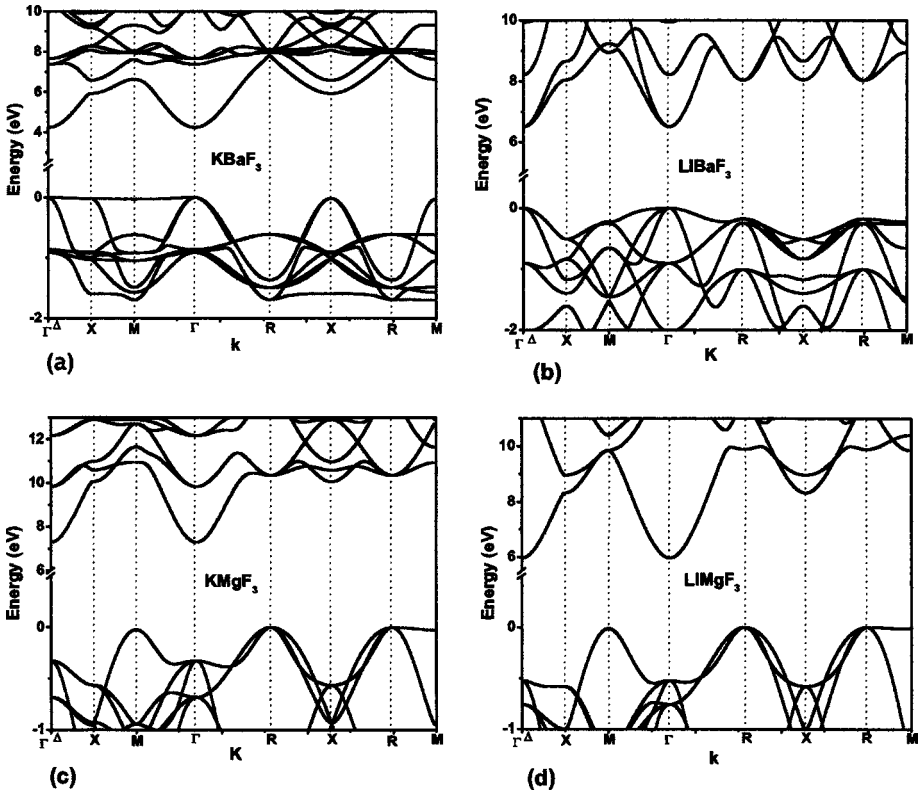

FIG. 2. Calculated band structure of (a) $KBaF_3$, (b) $LiBaF_3$, (c) $KMgF_3$, and (d) $LiMgF_3$. The valence-band maximum is set to 0 eV.

TABLE I. Band-gap energy, band structure, and lattice constant for $LiBaF_3$, $LiMgF_3$, $KBaF_3$, and $KMgF_3$.

Compound	Band gap (eV)	Calculated Γ Valley (eV)	Calculated R valley (eV)	Calculated Δ Valley (eV)	Lattice Constant (Å)	
					Literature data	Calculated data
$LiBaF_3$	6.513	6.513	6.685	6.516	3.994 (Ref. 20)	3.934
$LiMgF_3$	5.970	6.492	5.970	6.493	···	3.807
$KBaF_3$	4.243	4.244	4.855	4.243	···	5.002
$KMgF_3$	7.293	7.619	7.293	7.621	3.989 (Ref. 35)	3.928

$$E^{\Gamma,R,\Delta}_{Li_{(1-x)}K_xMgF_3} = E^{\Gamma,R,\Delta}_{KMgF_3}x + E^{\Gamma,R,\Delta}_{LiMgF_3}(1-x) - \frac{\alpha_{Li_{(1-x)}K_xMgF_3}}{\sqrt{\frac{E^{\Gamma,R,\Delta}_{KMgF_3} + E^{\Gamma,R,\Delta}_{LiMgF_3}}{2}}}x(1-x), \quad (2)$$

$$E^{\Gamma,R,\Delta}_{Li_{(1-x)}K_xBaF_3} = E^{\Gamma,R,\Delta}_{KBaF_3}x + E^{\Gamma,R,\Delta}_{LiBaF_3}(1-x) - \frac{\alpha_{Li_{(1-x)}K_xBaF_3}}{\sqrt{\frac{E^{\Gamma,R,\Delta}_{KBaF_3} + E^{\Gamma,R,\Delta}_{LiBaF_3}}{2}}}x(1-x), \quad (3)$$

and

$$\alpha_{Li_{(1-x)}K_xBa_{(1-y)}Mg_yF_3} = \alpha_{KBa_{(1-y)}Mg_yF_3}x + \alpha_{LiBa_{(1-y)}Mg_yF_3}(1-x), \quad (4)$$

α is a parameter that corresponds to the energy-gap sag, which is assumed to be 0.3, as proposed by Thompson and Woolley.[24] For the lattice constant of $Li_{(1-x)}K_xBa_{(1-y)}Mg_yF_3$, we assume that the variation follows Vegard's law

$$a_{Li_{(1-x)}K_xBa_{(1-y)}Mg_yF_3} = a_{LiBaF_3}(1-x)(1-y) + a_{KBaF_3}x(1-y) + a_{LiMgF_3}(1-x)y + a_{KMgF_3}xy. \quad (5)$$

It should be noted that for all the equations, the energy is expressed in eV and the lattice constant in angstrom. Both x and y coefficients obey the following conditions:

$$0 \leqslant x \leqslant 1,\ 0 \leqslant y \leqslant 1,\ \text{and}\ 0 \leqslant x+y \leqslant 1. \quad (6)$$

Since Δ and Γ band-gap energy values are almost similar, their evolution with respect to composition can be compared. Thus, only charts that show variations of Γ and R band-gap valleys are presented, and variations that correspond to the evolution of the Γ band-gap energy for $Li_{(1-x)}K_xBa_{(1-y)}Mg_yF_3$ versus composition are shown in Fig. 3. The chart is composed of infinite curves that correspond to compositions with equal band-gap energies. The borders of the chart represent the band-gap variation of the different binary compounds $Li_{(1-x)}K_xBaF_3$, $Li_{(1-x)}K_xMgF_3$, $LiBa_{(1-y)}Mg_yF_3$, and $KBa_{(1-y)}Mg_yF_3$. Figure 4 gives the variation of the R band-gap valleys as a function of $Li_{(1-x)}K_xBa_{(1-y)}Mg_yF_3$ composition. Based on Figs. 2–4, it is possible to determine a diagram that assembles the existing domains of the band-structure components Δ, Γ, and R, which correspond to $Li_{(1-x)}K_xBa_{(1-y)}Mg_yF_3$ compounds, as shown in Fig. 5. The plot illustrates the quaternary chart representing the variations of R, Δ and Γ band-gap valleys. The intersection between the equienergy curves R, Δ, and Γ traduce the existence of three distinct regions. One consists of $Li_{(1-x)}K_xBa_{(1-y)}Mg_yF_3$ compositions with a direct band gap, the Γ domain. The other two consist of compositions with indirect band gaps, the Δ and R domains. The thick solid lines in the plot represent the borders between either Δ and Γ or R and Γ domains. Compositions with equal lattice constants are represented by straight lines, which are called equilattice lines. Figure 6 represents an expanded portion of the $LiBaF_3$-rich part of the chart in Fig. 5. We can select direct band gap of $Li_{(1-x)}K_xBa_{(1-y)}Mg_yF_3$ compounds to design a double-heterostructure light-emitting diode (LED) or

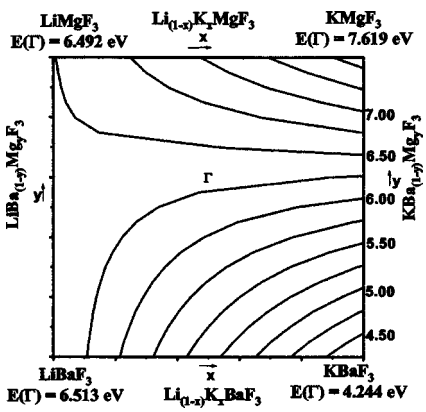

FIG. 3. Variation of the Γ-band structure of $Li_{(1-x)}K_xBa_{(1-y)}Mg_yF_3$ with respect to composition.

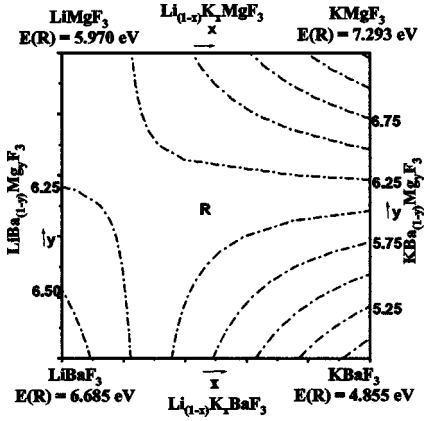

FIG. 4. Variation of the R-band structure of $Li_{(1-x)}K_xBa_{(1-y)}Mg_yF_3$ with respect to composition.

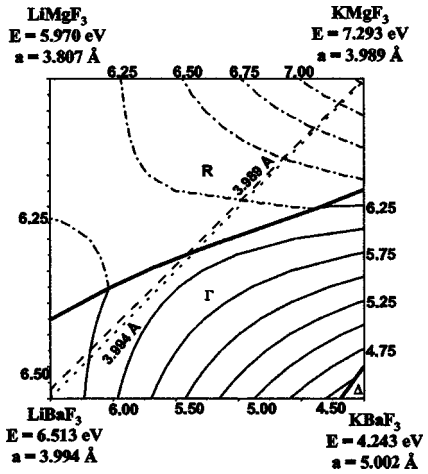

FIG. 5. Variations in the structure of band gap and lattice constants of $Li_{(1-x)}K_xBa_{(1-y)}Mg_yF_3$ with respect to composition. Thin solid and dash-dotted lines represent the equienergy gaps of Γ and R valleys, respectively. The thin-dotted and thin-dashed lines correspond to the equilattice constant lines $a=3.994$ and 3.989 Å, respectively. The borders between the direct and indirect band-gap domains, limit between either Γ and R or Γ and Δ domains, are marked as thick solid lines.

LD[25] that emits in the DUV range. In the following discussion, we propose $Li_{(1-x)}K_xBa_{(1-y)}Mg_yF_3$ perovskitelike superlattices and either $LiBaF_3$ or $KMgF_3$ as the substrate.

A. Design of $Li_{(1-x)}K_xBa_{(1-y)}Mg_yF_3/LiBaF_3$ superlattice structure

$Li_{(1-x)}K_xBa_{(1-y)}Mg_yF_3$ compounds that have a zero lattice mismatch ($f=0$ at room temperature) with $LiBaF_3$ are represented by the equilattice line with $a=3.994$ Å, the thin-dotted line in Fig. 5. The intersection between this equilattice line and the curve, which represents the border between the direct (Γ) and indirect (R) band-gap domains, corresponds to the lower limit of direct band-gap compounds with a lattice constant $a=3.994$ Å. This limit is equal to 6.111 eV, as shown with point *a* in Fig. 6. The composition $Li_{0.875}K_{0.125}Ba_{0.876}Mg_{0.124}F_3$, point *d*, is for the *n*-$LiBaF_3/Li_{0.875}K_{0.125}Ba_{0.876}Mg_{0.124}F_3/p$-$LiBaF_3$ double-heterostructure LD emitting at $\lambda=198$ nm (6.25 eV). Figure

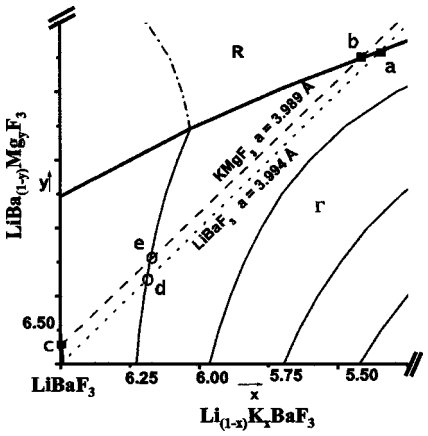

FIG. 6. Expanded fraction of the chart in Fig. 5 used to determine a suitable $Li_{(1-x)}K_xBa_{(1-y)}Mg_yF_3$ composition for a double-heterostructure photodiode or laser diode emitting in the DUV range.

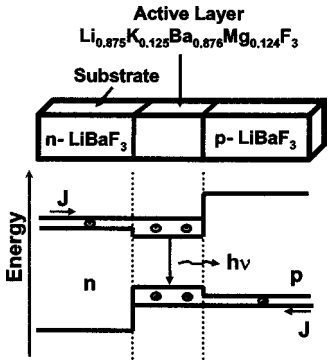

FIG. 7. Band-energy diagram of a double-heterostructure laser diode emitting at 6.25 eV ($\lambda=198$ nm) fabricated of $LiBaF_3/Li_{(1-x)}K_xBa_{(1-y)}Mg_yF_3$.

7 shows a schematic representing the structure principle for such a diode and the corresponding band-energy diagram. This structure will be sufficient for LED. With the appropriate cavity design, LD could also be feasible. For a more detailed design, the band offset parameter should also be considered.

B. Design of $Li_{(1-x)}K_xBa_{(1-y)}Mg_yF_3/KMgF_3$ superlattice structure

The $Li_{(1-x)}K_xBa_{(1-y)}Mg_yF_3$ compounds that possess $f=0$ with $KMgF_3$ are represented by the equilattice line with $a=3.989$ Å, the thin-dashed line in Fig. 5. The direct band-gap limit is between 6.117 and 6.506 eV as depicted by points *b* and *c* in Fig. 6. The composition $Li_{0.870}K_{0.130}Ba_{0.847}Mg_{0.153}F_3$, point *e*, can also be used to design *n*-$KMgF_3/Li_{0.805}K_{0.130}Ba_{0.847}Mg_{0.153}F_3/p$-$KMgF_3$, a double-heterostructure LD that emits at $\lambda=198$ nm (6.25 eV). Figure 8 shows the calculated band-gap offset of $LiBaF_3$ and $KMgF_3$ samples. By comparing with the widely known III-IV semiconductor diodes made from GaAs and AlAs, the lattice mismatches of $KMgF_3/LiBaF_3$ and GaAs/AlAs are equal to 1.25% and 1.27%, respectively. The low lattice mismatch *f* and Fig. 8 indicate that it is feasible to fabricate the superlattice $LiBa_{0.972}Mg_{0.027}F_3/KMgF_3$ with

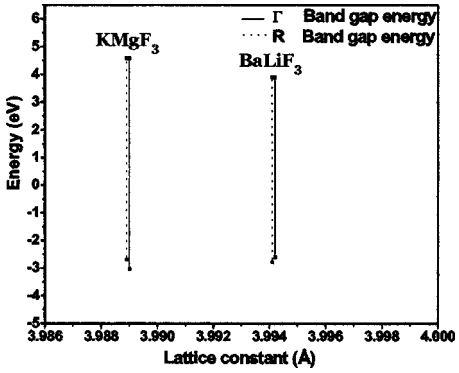

FIG. 8. The calculated band offset of $LiBaF_3$ and $KMgF_3$. The values shown at the top correspond to the conduction-band minimum while those shown at the bottom correspond to the valence-band maximum. For each sample, Γ and R valleys correspond to an identical lattice constant. For better representation, R valleys are slightly shifted with respect to the Γ valleys.

type I, and it will have quantum wells in both the valence and conduction bands. This photodiode could operate at $\lambda = 190$ nm (6.506 eV).

When considering the setup of this type of double-heterostructure LD, effort should be furnished with respect to deposition, cation substitution,[26] and doping of perovskite-like fluoride thin films. Although several papers reported the deposition of fluorides, such as CaF_2 (Ref. 27) and BaF_2,[28] few methods have been reported that successfully synthesized the perovskite fluorides.[29] Concerning the doping, the *n*-type perovskite fluorides are available and can be fabricated using the micro pulling down or the Czochralski method.[30] In an analogous approach applied for GaN, diamond, and ZnO,[11–13,31–33] the synthesis of *p*-type-doped fluorides should be investigated.

IV. CONCLUSION

In summary, this research suggests various possibilities for fluoride superlattices in optical applications as proposed for III-V compound semiconductors by Esaki and Tsu thirty years ago.[34] The results demonstrate the possibility of an elaborate design of either a light emitting diode or a laser diode that emit at wavelengths in the deep ultraviolet region. For emission at $\lambda = 198$ nm, the double-heterostructures *n*-$LiBaF_3/Li_{0.875}K_{0.125}Ba_{0.876}Mg_{0.124}F_3$/*p*-$LiBaF_3$ and *n*-$KMgF_3/Li_{0.805}K_{0.130}Ba_{0.847}Mg_{0.153}F_3$/*p*-$KMgF_3$ are proposed. The suggested photodiode $LiBa_{0.972}Mg_{0.027}F_3/KMgF_3$ could operate at $\lambda = 190$ nm. The next target of our research will be the deposition of thin films and the doping of the determined compounds.

[1]N. Sarukura, K. Hata, T. Adachi, R. Nodomi, M. Watanabe, and S. Watanabe, Phys. Rev. A **43**, 1669 (1991).
[2]T. Ariga, R. Nohdomi, and K. Hotta, Jpn. J. Appl. Phys., Part 1 **42**, 4325 (2003).
[3]M. Kaku, T. Higashiguchi, S. Kubodera, and W. Sasaki, Opt. Lett. **28**, 804 (2003).
[4]C. T. Chen, Y. B. Wang, B. C. Wu, K. C. Wu, W. L. Zeng, and L. H. Yu, Nature (London) **373**, 322 (1995).
[5]C. T. Chen, J. H. Lu, T. Togashi, T. Suganuma, T. Sekikawa, S. Watanabe, Z. Y. Xu, and J. Wang, Opt. Lett. **27**, 637 (2002).
[6]T. Kanai *et al.*, J. Opt. Soc. Am. B **21**, 370 (2004).
[7]M. A. Dubinskii, A. C. Cefalas, and C. A. Nicolaides, Opt. Commun. **88**, 122 (1992).
[8]E. Sarantopoulou, Z. Kollia, and A. C. Cefalas, Microelectron. Eng. **57–58**, 93 (2001).
[9]A. Sasaki, M. Nishiuma, and Y. Takeda, Jpn. J. Appl. Phys. **19**, 1695 (1980).
[10]M. A. Haase, J. Qiu, J. M. Depuydt, and H. Cheng, Appl. Phys. Lett. **59**, 1272 (1991).
[11]S. Nakamura, M. Senoh, and T. Mukai, Jpn. J. Appl. Phys., Part 2 **32**, L8 (1993).
[12]S. Koizumi, K. Watanabe, F. Hasegawa, and H. Kanda, Science **292**, 1899 (2001).
[13]H. Ohta, K. Kawamura, M. Orita, M. Hirano, N. Sarukura, and H. Hosono, Appl. Phys. Lett. **77**, 475 (2000).
[14]T. Sekiguchi and S. Koizumi, Appl. Phys. Lett. **81**, 1987 (2002).
[15]K. Horiuchi, A. Kawamura, T. Ide, T. Ishikura, K. Takamura, and S. Yamashita, Jpn. J. Appl. Phys., Part 2 **40**, L275 (2001).
[16]T. Nishimatsu, N. Terakubo, H. Mizuseki, Y. Kawazoe, D. A. Pawlak, K. Shimamura, and T. Fukuda, Jpn. J. Appl. Phys., Part 2 **41**, L365 (2002).
[17]K. Shimamura, N. Mujilatu, K. Nakano, S. L. Baldochi, Z. Liu, H. Ohtake, N. Sarukura, and T. Fukuda, J. Cryst. Growth **197**, 896 (1999).
[18]K. Shimamura, T. Fujita, H. Sato, A. Bensalah, N. Sarukura, and T. Fukuda, Jpn. J. Appl. Phys., Part 1 **39**, 6807 (2000).
[19]T. Fukuda, K. Shimamura, A. Yoshikawa, and E. G. Villora, Opto-Electron. Rev. **9**, 109 (2001).
[20]A. Bensalah, K. Shimamura, T. Fujita, H. Sato, M. Nikl, and T. Fukuda, J. Alloys Compd. **348**, 258 (2003).
[21]R. El Ouenzerfi *et al.*, Jpn. J. Appl. Phys., Part 2 **43**, L1140 (2004).
[22]K. Ohno, K. Esfarjani, and Y. Kawazoe, *Computational Materials Science: From Ab Initio to Monte Carlo Methods* (Springer, Berlin, 1999).
[23]C. Kittel, *Introduction to Solid-State Physics*, 6th ed. (Wiley, New York, 1986).
[24]A. G. Thompson and J. C. Woolley, Can. J. Phys. **45**, 255 (1967).
[25]I. Hayashi, M. B. Panish, P. W. Foy, and S. Sumski, Appl. Phys. Lett. **17**, 109 (1970).
[26]T. Nishimatsu, N. Terakubo, H. Mizuseki, Y. Kawazoe, D. A. Pawlak, K. Shimamura, N. Ichinose, and T. Fukuda, Jpn. J. Appl. Phys., Part 1 **42**, 5082 (2003).
[27]K. Adachi, T. Yao, T. Taniuchi, A. Kasuya, R. H. Miles, S. Uda, and T. Fukuda, Jpn. J. Appl. Phys., Part 2 **35**, L435 (1996).
[28]W. K. Liu, X. M. Fang, W. L. Yuan, M. B. Santos, T. Chatterjee, P. J. McCann, and E. A. Orear, J. Cryst. Growth **167**, 111 (1996).
[29]P. C. Burns, F. C. Hawthorne, A. M. Hofmeister, and S. L. Moret, Phys. Chem. Miner. **23**, 141 (1996).
[30]S. L. Baldochi, K. Shimamura, K. Nakano, N. Mujilatu, and T. Fukuda, J. Cryst. Growth **200**, 521 (1999).
[31]T. Yamamoto and H. Katayama-Yoshida, Physica B **302**, 155 (2001).
[32]A. Tsukazaki *et al.*, Appl. Phys. Lett. **81**, 235 (2002).
[33]M. Joseph, H. Tabata, and T. Kawai, Jpn. J. Appl. Phys., Part 2 **38**, L1205 (1999).
[34]L. Esaki and R. Tsu, IBM J. Res. Dev. **14**, 61 (1970).
[35]V. Luaña, A. Costales, and A. M. Pendas, Phys. Rev. B **55**, 4285 (1997).